One-pot synthesis of *in-situ* carbon-coated Fe_3O_4 as a long-life lithium-ion battery anode

To cite this article: Min Liu *et al* 2017 *Nanotechnology* **28** 155603

IOP Publishing Nanotechnology
Nanotechnology 28 (2017) 155603 (9pp) https://doi.org/10.1088/1361-6528/aa6143

One-pot synthesis of *in-situ* carbon-coated Fe_3O_4 as a long-life lithium-ion battery anode

Min Liu[1], Hongyun Jin[1,5], Evan Uchaker[2], Zhiqiang Xie[3], Ying Wang[3], Guozhong Cao[2], Shuen Hou[1] and Jiangyu Li[4,5]

[1] Faculty of Materials Science & Chemistry, China University of Geosciences, Wuhan, 430074, People's Republic of China
[2] Department of Materials Science & Engineering, University of Washington, Seattle, WA, 98195, United States of America
[3] Department of Mechanical Industrial Engineering, Louisiana State University, Baton Rouge, LA, 70803, United States of America
[4] Department of Mechanical Engineering, University of Washington, Seattle, WA, 98195, United States of America

E-mail: jinhongyun@cug.edu.cn and jjli@uw.edu

Received 8 December 2016, revised 20 January 2017
Accepted for publication 9 February 2017
Published 16 March 2017

Abstract

Fe_3O_4 has been regarded as a promising anode material for lithium-ion batteries (LIBs) due to its high theoretical capacity, low cost, and environmental friendliness. In this work, we present a one-pot reducing-composite-hydroxide-mediated (R-CHM) method to synthesize *in situ* carbon-coated Fe_3O_4 (Fe_3O_4@C) at 280 °C using $Fe(NO_3)_3 \cdot 9H_2O$ and PEG800 as raw materials and NaOH/KOH as the medium. The as-prepared Fe_3O_4 octahedron has an average size of 100 nm in diameter, covered by a carbon layer with a thickness of 3 nm, as revealed by FESEM and HRTEM images. When used as anode materials in LIBs, Fe_3O_4@C exhibited an outstanding rate capability (1006, 918, 825, 737, 622, 455 and 317 mAh g^{-1} at 0.1, 0.2, 0.5, 0.8, 1.0, 1.5 and 2.0 A g^{-1}). Moreover, it presented an excellent cycling stability, with a retained capacity of 261 mAh g^{-1} after 800 cycles under an extremely high specific current density of 2.0 A g^{-1}. Such results indicate that Fe_3O_4@C can provide a new route into the development of long-life electrodes for future rechargeable LIBs. Importantly, the R-CHM developed in our work can be extended for the synthesis of other carbon-coated electrodes for LIBs and functional nanostructures for broader applications.

Supplementary material for this article is available online

Keywords: carbon-coated Fe_3O_4, R-CHM method, long-life, anode

(Some figures may appear in colour only in the online journal)

Introduction

Lithium-ion batteries (LIBs) have been widely considered as one of the most promising energy storage/conversion systems to fulfil the growing energy demand of the global economy [7, 19, 24, 34, 35]. A high reversible capacity, long cycle stability, fast charge/discharge rate, and environment friendliness are the basic requirements of the ideal electrode materials for LIBs applications [21, 25, 27, 36]. In order to satisfy these requirements, recent research focus has been shifted from a graphitic anode with a theoretical capacity of 372 mAh g^{-1} to transition metal oxides with a higher specific capacity, such as Co_3O_4, Fe_3O_4, Fe_2O_3, SnO_2, CuO, MnO_2 and TiO_2 [4, 8, 12, 14, 22, 28, 37]. Iron oxides, such as α-Fe_2O_3 and Fe_3O_4, have been extensively investigated as potential electrode materials. Furthermore, Fe_3O_4—possessing a high theoretical specific capacity of 924 mAh g^{-1}, low cost, and environmental friendliness—is particularly attractive [13, 30, 38, 50]. Nevertheless, because of its lower electronic conductivity and large volume variation during

[5] Author to whom any correspondence should be addressed.

charging/discharging, poor cycling stability is still a serious issue that needs to be overcome before Fe_3O_4 can be used as a commercial anode material in LIBs [31, 46].

To mitigate the above predicament, carbon coatings have been explored to improve the performance of Fe_3O_4 anodes [26, 39, 42]. Studies have shown that coating carbon can not only facilitate ion and electron transports, but also relieve mechanical stress during the Li-ion insertion/extraction process. Various carbon coated Fe_3O_4 spheres, nanosheets, nanocubes, nanorods, pomegranate and sheaf-like structures have been successfully synthesized and they were found to possess improved electrochemical performances compared to a bare Fe_3O_4 electrode [2, 6, 45]. Thus, combining nanostructured Fe_3O_4 and a carbon matrix could be a promising way to optimize the electrochemical performance of an Fe_3O_4-based electrode, improve its cycling stability and prolonging its service life in LIBs [43, 44]. Recently, Zhao *et al* proposed a method of pyrolysis of polydopamineen capsulated carbonate crystals to synthesize an Fe_3O_4@C hybrid, which possesses a high reversible capacity of 770 $mAhg^{-1}$ at 200 mAg^{-1} after 50 cycles. In this method, the Fe_2CO_3 precursor was synthesized first, then the Fe_3O_4@C hybrid was obtained after pyrolysis at 500 °C [51]. Han *et al* reported hierarchically structured Fe_3O_4@C nanotubes prepared by three steps, which delivered a reversible capacity of 840 mAh g^{-1} at 1000 mA g^{-1} after 300 cycles. MoO_3 nanorods and FeOOH nanotubes were synthesized first and then calcined at 500 °C for 4 h to obtain Fe_3O_4@C nanotubes [10]. Ma *et al* prepared a sheaf-like hierarchical Fe_3O_4@C nanostructure by a facile solvothermal method, which exhibited a reversible capacity of 849 mAh g^{-1} at 500 mA g^{-1} over 200 cycles. In this process, $Fe(NO_3)_3 \cdot 6H_2O$ and glucose were heated at 220 °C first and then calcined at 350 °C for 3 h in N_2 gas [33]. Zhang *et al* proposed microwave irradiation as a heat source and Fe_3O_4/graphene composites were synthesized by depositing Fe^{3+} in the interspaces of graphene sheets. To obtain Fe_3O_4/graphene composites, GO was prepared by a modified Hummers' method, and then a mixture of GO, $Fe(NO_3)_3$ urea and ascorbic acid were refluxed under ambient conditions for 1 h and microwave heated, and finally, MGCs were obtained by treating the above products in an Ar atmosphere at 873 K for 8 h [48]. However, most of these methods used to synthesize the Fe_3O_4@C nanostructure have some disadvantages, including specific organic reagents, complicated experimental processes involving two or more steps, a high reaction temperature (mostly more than 280 °C) and poor reproducibility. Therefore, it is highly desirable to synthesize a carbon coated Fe_3O_4 nanostructure by a one step process.

Herein, we developed a reducing-composite-hydroxide-mediated (R-CHM) method to obtain the *in situ* carbon coated Fe_3O_4 (Fe_3O_4@C) using $Fe(NO_3)_3 \cdot 9H_2O$ and polyethylene glycol-800 (PEG800) as raw materials and NaOH/KOH (MOH) as a medium at 280 °C in one step. When used as an anode for LIBs, such Fe_3O_4@C possessed an exceptional capacity of 1006 mAh g^{-1} at a current density of 0.1 A g^{-1}. Moreover, the reversible capacities of 268 mAh g^{-1} can still be retained after 800 cycles under a high current density of 2.0 A g^{-1}.

Experimental section

Chemicals

$Fe(NO_3)_3 \cdot 9H_2O$, KOH, NaOH, and PEG800 were of analytical grade and were purchased from Sigma-Aldrich, with 99.9% purity. Deionized water was used in all the experimental processes.

Synthesis

Fe_3O_4@C was synthesized by the R-CHM method via the following steps. (1) First, 5.15 g of NaOH, 4.85 g of KOH and 1.2 g of $Fe(NO_3)_3 \cdot 9H_2O$ were mixed in a mortar and fully ground. (2) Then 0 or 5 g of PEG800 were added to the mixture, and were further ground. (3) Two mixtures were put into a 25 ml Teflon container, placed in an electric oven and heated at 280 °C for 48 h. (4) The Teflon container was taken out and cooled to room temperature naturally after reaching the specified time. (5) The precipitate formed in the container was washed with deionized water and ethanol until the pH value reached 7, and then dried in vacuum. The sample obtained with 0 g PEG800 was labelled as S_1, while the other one was labelled S_2.

Characterizations

X-ray diffraction (XRD) analysis was carried out using nickel filtered Cu Kα radiation on a Bruker D8 Advance diffractometer to identify the crystalline phase of the as-prepared samples. The morphology was characterized by an SU8010 field emission scanning electron microscope (FE-SEM) and D8-high resolution transmission electron microscopy (HR-TEM). The reaction mechanism in the R-CHM method was analyzed via a thermo-gravimetric differential scanning calorimeter (TG–DSC) (STA449C/3/G) with a heating rate of 10 °C min^{-1}. Fourier transform infrared spectroscopy (FT-IR) was performed to analyze the surface characteristics of PEG800 and the intermediates in the reaction system by a SHIMAUZU-8400 system. The specimens were mixed with KBr pellets and then pressed into a pelletizer for FT-IR measurements. Magnetic measurements were performed by a Lake Shore 7410 vibrating sample magnetometer (VSM) operated at room temperature. The magnetic hysteresis loop was measured in the field range between $\pm$10 kOe at room temperature.

Electrochemical measurements

For electrochemical analysis, coin-type half cells (CR 2025) were assembled in a glove box filled with high purity argon. The anode was prepared by mixing 80 wt% of the active material (e.g. Fe_3O_4@C), 10 wt% of Super P conductive carbon, and 10 wt% of polyvinylidene fluoride binder in *N*-methyl pyrrolidone solvent on copper foil. It was then put into

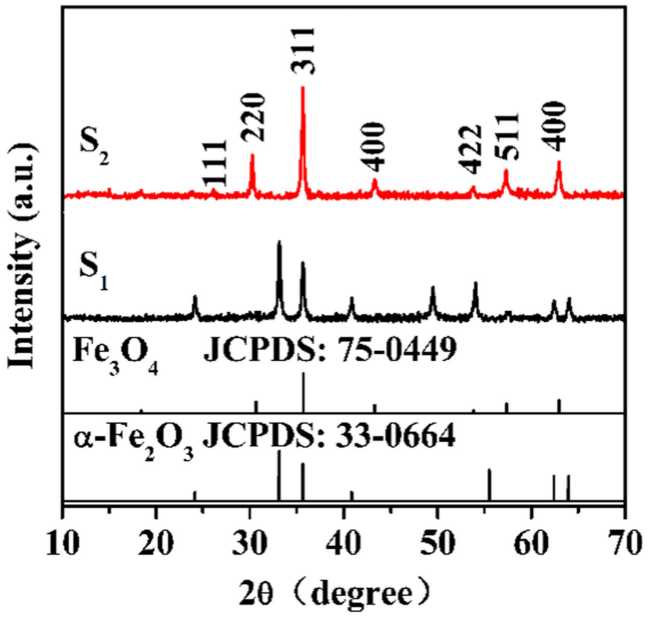

Figure 1. XRD patterns of S_1 (α-Fe_2O_3) and S_2 (Fe_3O_4@C).

a vacuum oven and dried at 120 °C for 12 h. The copper foils coated with active materials were cut into circular sheets with a diameter of 1.33 cm and assembled in the glove box. Lithium (Li) metal was used as the cathode and the complex of ethyl methyl carbonate, 1 M $LiPF_6$ in dimethyl carbonate and ethylene carbonate (1:1:1, v/v/v) was used as an electrolyte, and the Celgard 2400 as a separator. Cyclic voltammetry (CV) was carried out between 0.01 and 3.0 V versus Li/Li^+ at scanning rates of 0.5 mV s^{-1} using an electrochemical analyzer (Solartron, 1260/1287). The current density and cycle stability were performed on an Arbin battery tester (BT-2000, Arbin Instruments) between 0.01 and 3.0 V versus Li/Li^+ at various charging rates of 0.1, 0.2, 0.5, 0.8, 1.0, 1.5 and 2.0 A g^{-1}. To validate the electrochemical kinetics of Fe_3O_4@C, electrochemical impedance spectroscopy (EIS) measurements were examined by a frequency response analyser (Solartron, 1260/1287) in the frequency range from 0.1 Hz–100 kHz with an AC signal amplitude of 10.0 mV.

Results and discussion

Figure 1 shows the XRD patterns of S_1 and S_2. The lower standard XRD pattern confirmed that all the diffraction peaks of S_1 can be assigned to the hexagonal phase of α-Fe_2O_3 (JCPDS No.33-0664) [53]. Meanwhile, the diffraction peaks of S_2 at $2\theta = 26.30°$, 30.01°, 35.41°, 43.11°, 53.61°, 56.91° and 62.41° were indexed to (111), (220), (311), (400), (422), (511) and (440)—in good agreement with the pure face-centred cubic Fe_3O_4 (JCPDS No. 75-0449) [5, 29]. This suggests that the α-Fe_2O_3 had completely transformed into the Fe_3O_4 after being heated to 280 °C for 48 h together with PEG800. All the diffraction peaks of S_2 were sharp in width and strong in intensity, indicating that it has excellent crystallinity, while there was no diffraction peak corresponding to carbon observed in the XRD pattern. FT-IR spectra of bare PEG800 (figure S1(a) is available at stacks.iop.org/NANO/28/155603/mmedia) and PEG800 reacting in MOH at 280 °C (figure S1(b)) have been obtained. As shown in figure S1, compared to bare PEG800, the absorption peaks of –OH and $–CH_2$ almost disappeared after PEG800 was reacted in MOH for some time, suggesting that PEG800 could be converted into carbon after prolonging the reaction time. Therefore, combining the XRD and FT-IR results, we suggested that PEG800 has transformed into carbon in the process of the synthesis of Fe_3O_4, which was confirmed by the subsequent TEM image.

In order to characterize the microstructures, FE-SEM, HR-TEM and SAED images of S_2 (Fe_3O_4@C) were examined. The FE-SEM image revealed the detailed morphology of Fe_3O_4@C, which showed an octahedral shape and uniform size (figure 2(a)). From the enlarged image in figure 2(b), it was found that Fe_3O_4 crystals have an octahedral morphology with eight facets and have a lateral size of 100 nm. With reference to the FE-SEM analysis above, the TEM images gave a further view of the octahedral Fe_3O_4@C nanostructure. The same selected area was presented in bright and dark fields, and is shown in figures 2(c) and (d). From the bright-field TEM image in figure 2(c), it can be seen that Fe_3O_4 possesses regular geometrical morphology, and thus good crystallization. From the dark-field TEM image in figure 2(d), it was observed that some bright spots were covered by shallow grey flocculent matter, suggesting that the surface of the Fe_3O_4 octahedron was coated with a layer of amorphous material, believed to be carbon. From the higher-magnification TEM image in figure 2(e), it can be seen that the Fe_3O_4 nanocrystals exhibited a regular octahedral shape and the entire surface of the Fe_3O_4 octahedron was covered by a uniform carbon layer to form a composite structure of Fe_3O_4@C. After further magnification, the carbon coating wrapping the Fe_3O_4 octahedron was revealed, as shown in figure 2(f). The thickness of the carbon was measured to be around 3 nm, as marked by the blue dashed lines in figure 2(f). The homogeneous carbon coating structure could effectively improve the conductivity of the electrodes, limit the volume change of Fe_3O_4 octahedron materials and keep the Fe_3O_4 electrode stable during Li^+ intercalation and deintercalation. Moreover, a small amount of lattice fringes can be observed in the local area. The lattice fringe pitch of 0.30 nm corresponds well with the *d*-spacing of the (220) reflections of Fe_3O_4 [17]. In addition, the relative SAED pattern (inset in figure 2(f)) disclosed rectangular bright diffraction spots, which can be indexed to the crystal planes (220) and (111) of Fe_3O_4, indicating the perfect single crystalline structure of the Fe_3O_4 nanocrystals [40]. At the same time, the morphology and structural characteristics of S_1 (α-Fe_2O_3) were examined by SEM and TEM as well, as shown in figure S2, revealing the as-synthesized α-Fe_2O_3 sample consisting of dispersed nanosheets that were hexagonal plates with an average diameter of 1 μm and a thickness of about 50 nm. The structures of Fe_3O_4@C and α-Fe_2O_3 were further supported by their magnetic properties measured using VSM

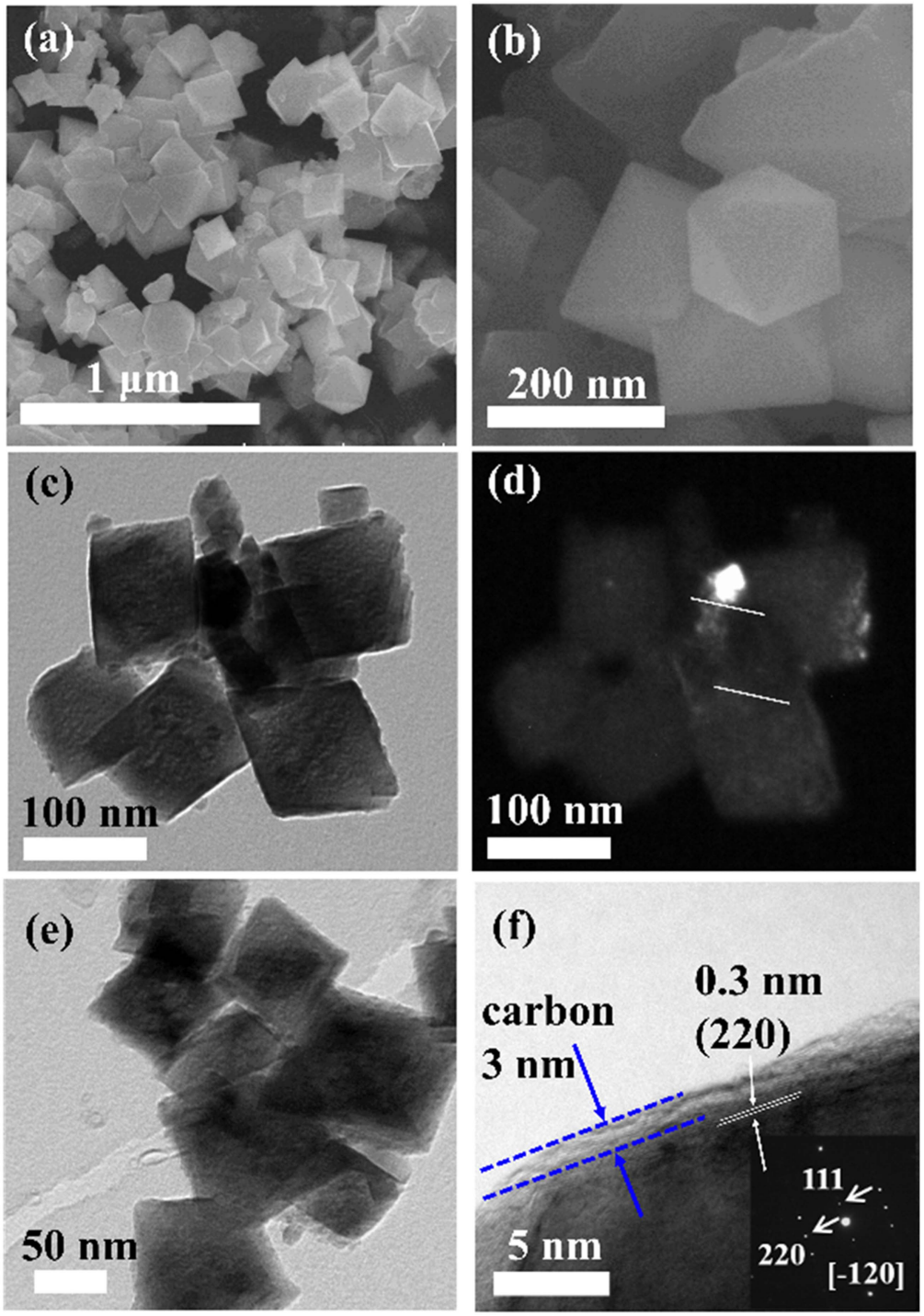

Figure 2. SEM, TEM, HRTEM, and SAED images of the Fe_3O_4@C nanostructure. (a) and (b) SEM images; (c) and (d) TEM images in the bright field and dark field; (e) and (f) high-magnification TEM images.

at room temperature, as shown in figure S3, confirming their ferromagnetic characteristics. The saturation magnetization of 26.8 emu g^{-1}, the remanent magnetization of 5.2 emu g^{-1} and the coercivity of 165.4 Oe measured in Fe_3O_4@C are smaller than values reported previously, which could be explained by the surface coating of the carbon layer on Fe_3O_4.

The reaction process of $Fe(NO_3)_3 \cdot 9H_2O$ and PEG800 in the MOH medium can be understood from the TG–DSC curves in figure 3. According to the DSC results, there were five endothermic peaks at 66 °C, 91 °C, 105 °C, 132 °C, and 261 °C, and one exothermic peak at 114 °C. The endothermic peak at 66 °C occurs with hardly any weight change, which was believed to correspond to $Fe(NO_3)_3 \cdot 9H_2O$ changed to $Fe(OH)_3$. The endothermic peaks at 91 °C and 105 °C were associated with a 1.2% weight loss, which was ascribed to the amount of adsorbed water that was lost from the heating process. At 114 °C, a sharp exothermic peak occurred with obvious weight loss, corresponding to the start of the PEG800

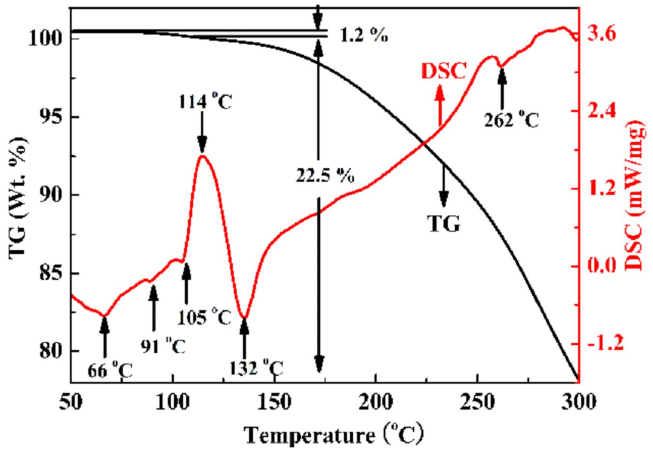

Figure 3. TG–DSC curves of the $Fe(NO_3)_3 \cdot 9H_2O$ and PEG800 decomposition in MOH medium.

decomposition. An endothermic peak appears at 132 °C, which was attributed to $Fe(OH)_3$ decomposition. Finally, an endothermic peak occurred at 262 °C corresponding to the carbon thermal reduction of Fe_2O_3 into Fe_3O_4. It should be pointed out that, during the process from 114 °C–300 °C, the weight loss was about 22.5%—much larger than the theoretical value of 3.8% for the weight loss associated with the decomposition of $Fe(NO_3)_3 \cdot 9H_2O$ into Fe_2O_3. This difference was likely caused by the weight loss associated with the gradual carbonization of PEG800. Combined with the XRD results above, it was thus concluded that PEG800 provided a reducing agent to transform Fe^{3+} into Fe^{2+} and thus form Fe_3O_4.

The detailed reaction mechanism during the R-CHM synthesis of Fe_3O_4@C is summarized by the following equations:

$$50\ ^\circ\text{C} \sim 100\ ^\circ\text{C}: Fe^{3+} + 3OH^- \rightarrow Fe(OH)_3 \quad (1)$$

$$100\ ^\circ\text{C} \sim 250\ ^\circ\text{C}: \text{PEG800} \rightarrow C + O_2 + H_2O \quad (2)$$

$$120\ ^\circ\text{C} \sim 200\ ^\circ\text{C}: Fe(OH)_3 \rightarrow Fe_2O_3 + H_2O \quad (3)$$

$$200\ ^\circ\text{C} \sim 300\ ^\circ\text{C}: Fe_2O_3 + C \rightarrow Fe_3O_4 + CO_2 \quad (4)$$

According to the above results of XRD, FESEM and TG–DSC, the formation mechanism of Fe_3O_4@C can be inferred. As illustrated in scheme 1, the Fe_3O_4@C was obtained by a simple one-pot method, as follows: (a) the raw mixture consisted of $Fe(NO_3)_3 \cdot 9H_2O$, PEG800, MOH that were mixed uniformly with full grinding; (b) after heating at 132 °C, the introduced PEG800 formed a carbon–oxygen skeleton by partial dehydration in the MOH medium, and $Fe(OH)_3$ decomposed to α-Fe_2O_3. The carbon–oxygen skeleton was then adsorbed on the surface of the obtained α-Fe_2O_3 nanosheets by a large number of hydroxyl groups; (c) when the temperature increased to 262 °C, the carbon–oxygen skeleton transformed to carbon molecules and the α-Fe_2O_3 was reduced to Fe_3O_4 by carbon molecules; the remaining carbon–oxygen skeleton was coated on the surface of octahedral Fe_3O_4; (d) as the reaction time progressed, the remaining carbon–oxygen skeleton transformed to carbon molecules and was coated on the surface of the Fe_3O_4 octahedron. As a result, a carbon coated octahedral Fe_3O_4

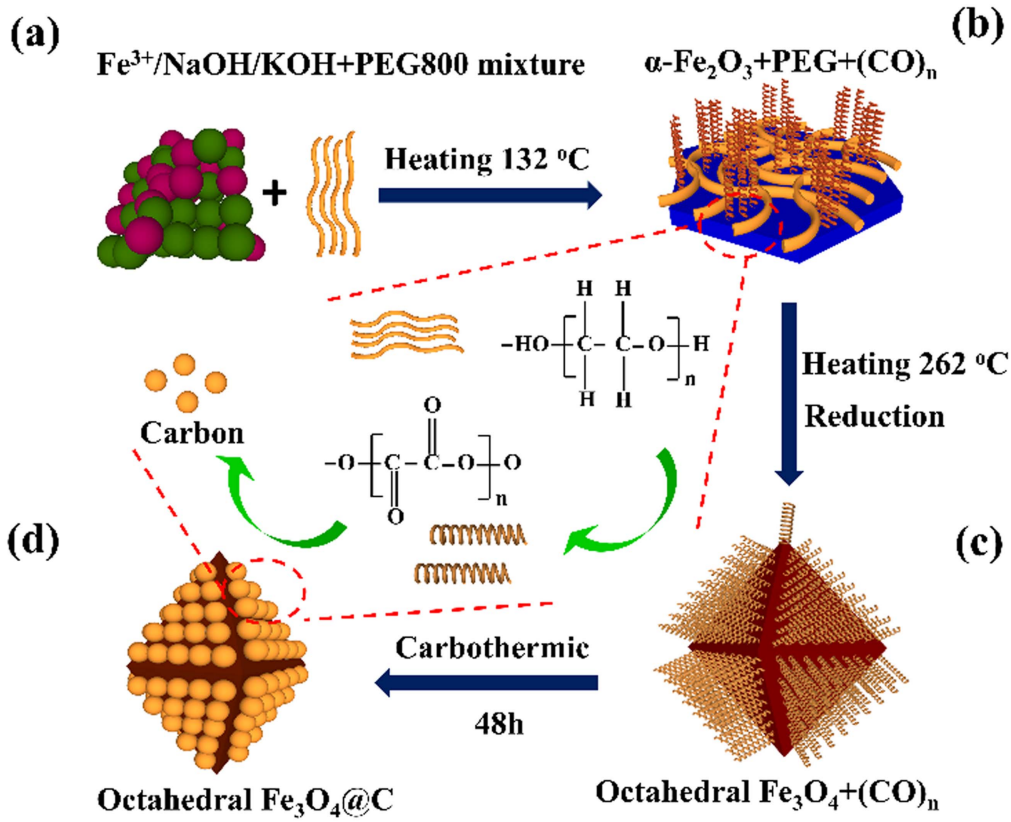

Scheme 1. Illustration of the assembly process and formation mechanism of Fe_3O_4@C.

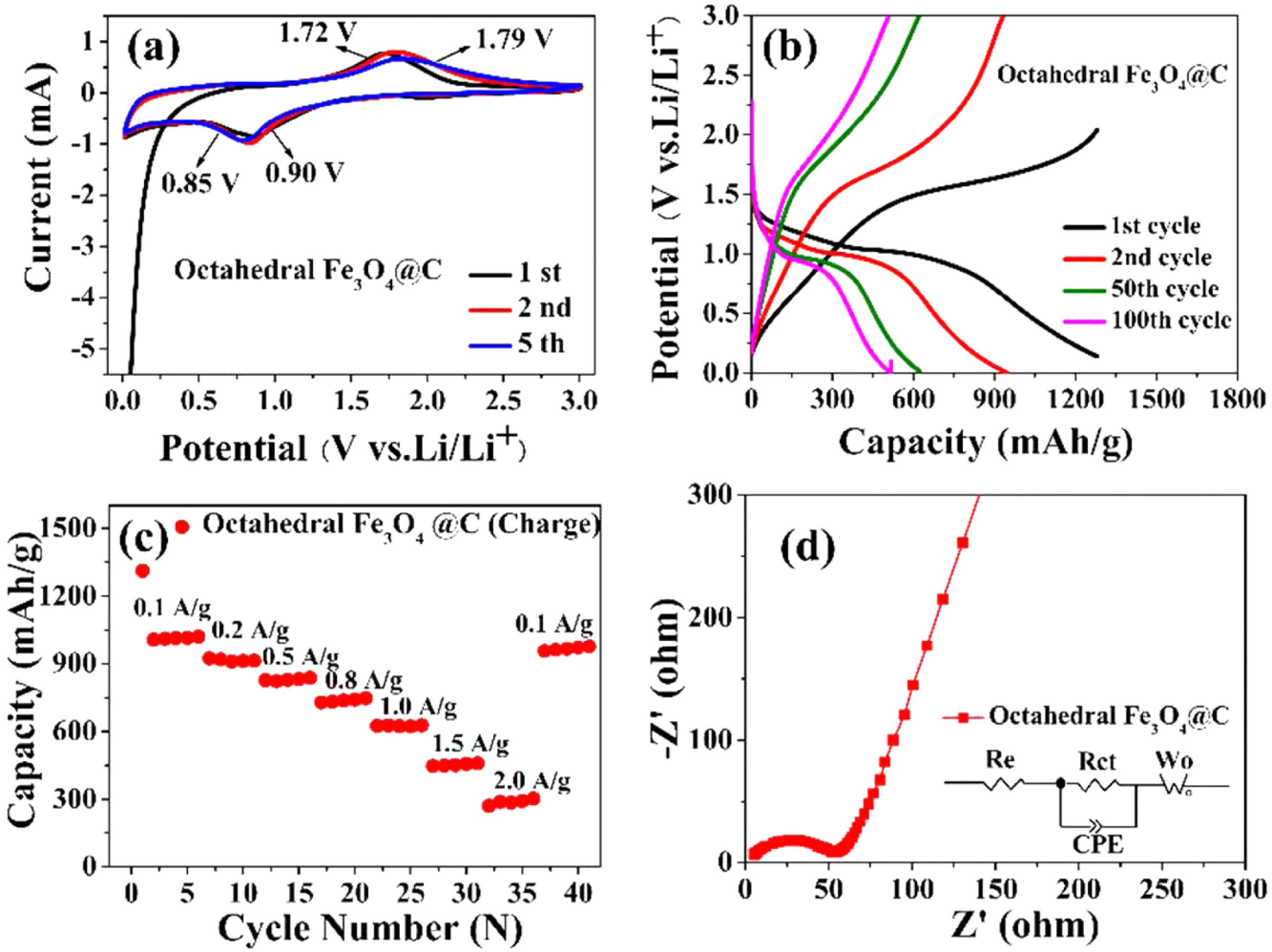

Figure 4. (a) Cyclic voltammograms of Fe_3O_4@C at a scan rate of 0.5 mVs^{-1} between 0.01 and 3.0 V; (b) discharge/charge profiles of Fe_3O_4@C for the initial 100 cycles at a specific current of 0.1 A g^{-1}; (c) the rate capabilities of Fe_3O_4@C at different specific currents between 0.1 and 2.0 A g^{-1}; (d) Nyquist plots of Fe_3O_4@C electrodes before electrochemical cycling by applying an AC voltage of 10 mV over the frequency range from 0.1 Hz–100 kHz.

nanostructure was obtained. The phase transition can be demonstrated by XRD, the morphological description can be obtained according to the FESEM images, and the reaction temperature is comfirmed by the TG–DSC results from (a) to (d).

The electrochemical properties of the Fe_3O_4@C were examined by CV and galvanostatic charge/discharge tests. The typical cyclic voltammograms of the Fe_3O_4@C anode in the initial three cycles between 0.01 V and 3.0 V at a scanning rate of 0.5 mVs^{-1} are shown in figure 4(a). In the first cathodic process, the major peaks located around 0.85 V could be attributed to the formation of Li_2O and solid electrolyte interface (SEI) film [11, 20]. Further, the anodic peak at 1.72 V demonstrated the extraction of Li from the electrode material. In the subsequent cycles, it could be seen that the cathodic peak at 0.85 V shifted to 0.90 V, which might be considered to enhance the physical buffering affect and increase the polarization of the electrode material after being coated with a layer of amorphous carbon. The peak at 1.72 V shifting to 1.79 V might be ascribed to the increased oxidation of Fe^0 to Fe^{3+} due to the formation of the carbon layer.

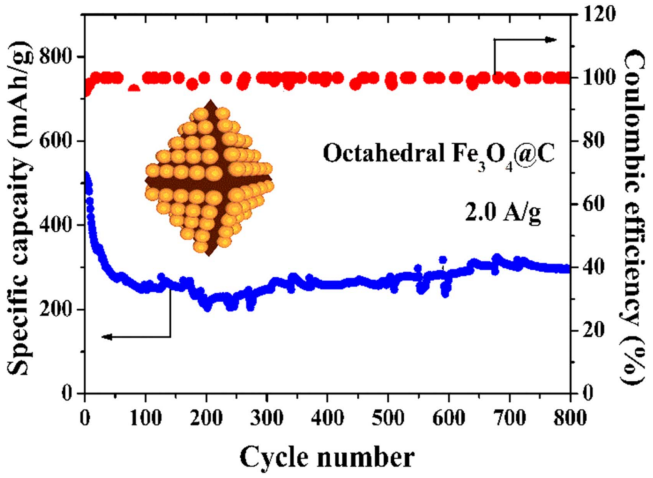

Figure 5. Cycling performance of Fe_3O_4@C at a specific current of 2.0 A g^{-1}.

Table 1. Comparison of the electrochemical performance for the iron oxides as anode materials of LIBs in the recently reported literature.

Materials	Synthesized steps	Current density	Charge capacity after cycling	Ref.
commercial Fe_3O_4 nanoparticles		0.1 C	70 mAh g^{-1} after 50 cycles	[48]
Fe_2O_3–GO	four steps	0.2 C	350 mAh g^{-1} after 100 cycles	[49]
MoO_2–GO	two steps	500 mA g^{-1}	310 mAh g^{-1} after 30 cycles	[12]
MnO/carbon	three steps	2000 mAg^{-1}	525 mAh g^{-1} after 1000 cycles	[16]
Fe_3O_4@C	three steps	0.2 C	543 mAh g^{-1} after 2000 cycles	[23]
Fe_3O_4@C	three steps	300 mAg^{-1}	254 mAh g^{-1} after 100 cycles	[28]
Fe_3O_4@C	one step	2000 mAg^{-1}	268 mAh g^{-1} after 800 cycles	this work

Figure 4(b) reveals the galvanostatic charge/discharge curves of the Fe_3O_4@C at 0.1 A g^{-1}. At 1.0 V, there was a distinct voltage plateau in the discharge curve that corresponds to Li^+ insertion into Fe_3O_4 and the formation of the SEI films after electrolyte decomposition [3, 10, 41]. A reversible conversion from Fe to Fe_3O_4 at a sloping plateau around 1.7 V was observed in the charge curve. The capacities during the first two cycles were measured to be 1297 mAh g^{-1} and 950 mAh g^{-1}. Furthermore, it was noted that a high reversible capacity of 630 mAh g^{-1} was achieved after 50 cycles. After 100 cycles, it still maintained a reversible capacity of 505 mAh g^{-1}. These results suggest that the integrity of Fe_3O_4@C could be retained during long-life cycles.

The rate capability of the as-prepared Fe_3O_4@C was tested at various specific currents ranging from 0.1–2.0 A g^{-1}. As shown in figure 4(c), at 0.1 Ag^{-1}, the stable capacity of Fe_3O_4@C was around 1006 mAh g^{-1}. When the specific current raised to 0.5 A g^{-1}, a stable high capacity of 825 mAh g^{-1} could be achieved. At a high specific current of 1.0 A g^{-1}, the Fe_3O_4@C could possess a stable capacity of 622 mAh g^{-1} (figure 4(c)). At an even higher specific current of 2.0 A g^{-1}, it presented a reversible capacity of 317 mAh g^{-1}. Remarkably, when the specific current was reduced back to 0.1 mA g^{-1} after 35 cycles, a stable high capacity of 1006 mAh g^{-1} could be recovered (figure 4(c)). Such enhanced electrode kinetics could be further examined by EIS measurements. The charge transport properties of the Fe_3O_4@C samples were measured by EIS at an open-circuit voltage of 2.85 V. As shown in figure 4(d), it was observed that from 10^2 Hz–10^5 Hz, the Nyquist plots displayed a depressed semicircle and from 0.1 Hz–10^2 Hz displayed a sloped line, which correspond to the charge transfer resistance (R_{ct}) and Warburg impedance (W_o), respectively [1, 42]. The value of the charge transfer resistance (R_{ct}) was 52 Ω for Fe_3O_4@C, indicating the significantly improved charge transport properties of the Fe_3O_4@C electrode due to the presence of the carbon layer on its surface.

To verify the long-term cycling stability and high rate capability of Fe_3O_4@C as an anode material for LIBs, it was tested at an extremely high specific current of 2.0 A g^{-1} for 800 cycles, as shown in figure 5. It can be seen that the reversible capacity was stabilized around 300 mAh g^{-1} at the 50th cycle and the capacity decay ratio was about 58%. After 800 cycles, the Fe_3O_4@C anode remained at a reversible capacity of 268 mAh g^{-1} and the capacity decay ratio was about 52%. It is noted that the capacity decreased at the start of the 50 cycles. This phenomenon has also been observed in previous researches [15, 32, 52]. The possible reason is that when the current density is too large, the anode is prone to polarization which causes Li ion reduction by deposition. So the capacity decreased in the initial stage [32]. The excellent cycling stability and rate performance of Fe_3O_4@C may be attributed to the synergic effects of each component in the composite [18]. Firstly, the nanosize octahedral Fe_3O_4 can significantly increase the electrode/electrolyte contact area and shorten the electron and Li ion diffusion distances; secondly, the carbon coating can effectively improve the structural stability of the electrode by suppressing the aggregation of the Fe_3O_4 octahedron and accommodating its volume expansion during the process of charge/discharge [9, 47]. Moreover, to verify the long-term cycling stability, the performance of other similar materials reported in the literature are summarized in table 1. It can be seen that the Fe_3O_4@C exhibited a long-term cycling stability when synthesized by the R-CHM method. All the above characteristics proved Fe_3O_4@C to be a promising anode material for high performance LIBs.

Conclusion

A novel one-pot R-CHM strategy was developed for the synthesis of an octahedral Fe_3O_4@C nanostructure at 280 °C. Such Fe_3O_4@C delivered reversible capacities of 1006–317 mAh g^{-1} over a wide range of specific currents of 0.1–2.0 A g^{-1}. Importantly, it maintained a reversible capacity of 268 mAh g^{-1} after 800 cycles at 2.0 A g^{-1}. These excellent electrochemical properties are attributed to the uniform-sized octahedral Fe_3O_4 and *in situ* carbon coating. The carbon layer on the surface of the octahedral Fe_3O_4 could effectively improve the electrode conductivity, avoid direct exposure of the Fe_3O_4 octahedral to the electrolyte and help to reduce the mechanical stress during the Li-ion insertion/extraction process. Therefore, this R-CHM method is an ideal one-step technique to obtain an *in situ* carbon coating structure at lower temperatures. Thanks to its facility and versatility, the R-CHM method invented in our work can be extended to the synthesis of other functional nanostructures for various applications.

Acknowledgments

This work was financially supported in part by the National Key Research Program of China (2016YFA0201001), the National Nature Science Foundation of China (NSFC51102218), the National Science Foundation (NSF, DMR-1505902), the National Natural Science Foundation of China (11627801), and the Shenzhen Science and Technology Innovation Committee (ZDSYS20140509162754023).

References

[1] Bi N, Liu X, Wu N, Cui C and Sun Y 2015 Improved electrochemical performance of onion-like carbon coated magnetite nanocapsules as electromagnetic absorptive anode materials for lithium-ion batteries *RSC Adv.* **5** 32452–9

[2] Cao H, Liang R, Qian D, Shao J and Qu M 2011 L-Serine-assisted synthesis of superparamagnetic Fe_3O_4 nanocubes for lithuium ion batteries *J. Phys. Chem.* C **115** 24688–95

[3] Chai X, Shi C, Liu E, Li J, Zhao N and He C 2015 Carbon-coated Fe_2O_3 nanocrystals with enhanced lithium storage capability *Appl. Surf. Sci.* **347** 178–85

[4] Chen K and Xue D 2013 Room-temperature chemical transformation route to CuO nanowires toward high-performance electrode materials *J. Phys. Chem.* C **117** 22576–83

[5] Chen M, Shen X, Chen K, Wu Q, Zhang P, Zhang X and Diao G 2016 Nitrogen-doped mesoporous carbon-encapsulation urchin-like Fe_3O_4 as anode materials for high performance li-ions batteries *Electrochim. Acta* **195** 94–105

[6] Cheng X-L, Jiang J-S, Jiang D-M and Zhao Z-J 2014 Synthesis of rhombic dodecahedral Fe_3O_4 nanocrystals with exposed high-energy {110} facets and their peroxidase-like activity and lithium storage properties *J. Phys. Chem.* C **118** 12588–98

[7] Ding Y-L, Kopold P, Hahn K, van Aken P A, Maier J and Yu Y 2016 Facile solid-state growth of 3D well-interconnected nitrogen-rich carbon nanotube-graphene hybrid architectures for lithium-sulfur batteries *Adv. Funct. Mater.* **26** 1112–9

[8] Fan X, Shao J, Xiao X, Wang X, Li S, Ge H, Chen L and Wang C 2014 *In situ* synthesis of SnO_2 nanoparticles encapsulated in micro/mesoporous carbon foam as a high-performance anode material for lithium ion batteries *J. Mater. Chem.* A **2** 18367–74

[9] Geng H B, Zhou Q, Zheng J W and Gu H W 2014 Preparation of porous and hollow Fe_3O_4@C spheres as an efficient anode material for a high-performance Li-ion battery *RSC Adv.* **4** 6430–4

[10] Han F, Ma L, Sun Q, Lei C and Lu A 2014 Rationally designed carbon-coated Fe_3O_4 coaxial nanotubes with hierarchical porosity as high-rate anodes for lithium ion batteries *Nano Res.* **7** 1706–17

[11] Harada K *et al* 2016 Electrochemical reactions and cathode properties of Fe-doped Li_2O for the hermetically sealed lithium peroxide battery *J. Power Sources* **322** 49–56

[12] Hu S, Yin F, Uchaker E, Chen W, Zhang M, Zhou J, Qi Y and Cao G 2014 Facile and green preparation for the formation of MoO_2-GO composites as anode material for lithium-ion batteries *J. Phys. Chem.* C **118** 24890–7

[13] Hu X *et al* 2014 Supercritical carbon dioxide anchored Fe_3O_4 nanoparticles on graphene foam and lithium battery performance *ACS Appl. Mater. Interfaces* **6** 22527–33

[14] Huang G, Xu S, Lu S, Li L and Sun H 2014 Micro-/nanostructured Co_3O_4 anode with enhanced rate capability for lithium-ion batteries *ACS Appl. Mater. Interfaces* **6** 7236–43

[15] Huang X, Chen J, Lu Z, Yu H, Yan Q and Hng H H 2013 Carbon inverse opal entrapped with electrode active nanoparticles as high-performance anode for lithium-ion batteries *Sci. Rep.* **3** 02317

[16] Jiang H, Hu Y, Guo S, Yan C, Lee P S and Li C 2014 Rational design of MnO/carbon nanopeapods with internal void space for high-rate and long-life li-ion batteries *ACS Nano* **8** 6038–46

[17] Jiang X, Yang X, Zhu Y, Yao Y, Zhao P and Li C 2015 Graphene/carbon-coated Fe_3O_4 nanoparticle hybrids for enhanced lithium storage *J. Mater. Chem.* A **3** 2361–9

[18] Jo M R *et al* 2016 Fe_3O_4 nanoparticles encapsulated in one-dimensional $Li_4Ti_5O_{12}$ nanomatrix: an extremely reversible anode for long life and high capacity Li-ion batteries *Nano Energy* **19** 246–56

[19] Kim H *et al* 2016 Enhancing interfacial bonding between anisotropically oriented grains using a glue-nanofiller for advanced li-ion battery cathode *Adv. Mater.* **28** 4705–12

[20] Kobayashi H *et al* 2016 Improved performance of Co-doped Li_2O cathodes for lithium-peroxide batteries using $LiCoO_2$ as a dopant source *J. Power Sources* **306** 567–72

[21] Koo B, Xiong H, Slater M D, Prakapenka V B, Baasubramanian M, Podsiadlo P, Johnson C S, Rajh T and Shevchenko E V 2012 Hollow iron oxide nanoparticles for application in lithium ion batteries *Nano Lett.* **12** 2429–35

[22] Lang L and Xu Z 2013 *In situ* synthesis of porous Fe_3O_4/C microbelts and their enhanced electrochemical performance for lithium-ion batteries *ACS Appl. Mater. Interfaces* **5** 1698–703

[23] Li D, Li X, Wang S, Zheng Y, Qiao L and He D 2014 Carbon-wrapped Fe_3O_4 nanoparticle films grown on nickel foam as binder-free anodes for high-rate and long-life lithium storage *ACS Appl. Mater. Interfaces* **6** 648–54

[24] Li F, Chen H, Liu X Y, Zhu S J, Jia J Q, Xu C H, Dong F, Wen Z Q and Zhang Y X 2016 Low-cost high-performance asymmetric supercapacitors based on Co_2AlO_4@MnO_2 nanosheets and Fe_3O_4 nanoflakes *J. Mater. Chem.* A **4** 2096–104

[25] Li W, Yang Z, Li M, Jiang Y, Wei X, Zhong X, Gu L and Yu Y 2016 Amorphous red phosphorus embedded in highly ordered mesoporous carbon with superior lithium and sodium storage capacity *Nano Lett.* **16** 1546–53

[26] Li X *et al* 2012 Tin oxide with controlled morphology and crystallinity by atomic layer deposition onto graphene nanosheets for enhanced lithium storage *Adv. Funct. Mater.* **22** 1647–54

[27] Liu C, Neale Z G and Cao G 2016 Understanding electrochemical potentials of cathode materials in rechargeable batteries *Mater. Today* **19** 109–23

[28] Liu J, Ni J, Zhao Y, Wang H and Gao L 2013 Grapecluster-like Fe_3O_4@C/CNT nanostructures with stable Li-storage capability *J. Mater. Chem.* A **1** 12879–84

[29] Liu J, Xu X, Hu R, Yang L and Zhu M 2016 Uniform hierarchical Fe_3O_4@polypyrrole nanocages for superior lithium ion battery anodes *Adv. Energy Mater.* **6** 1600256

[30] Liu L, Yang X, Lv C, Zhu A, Zhu X, Guo S, Chen C and Yang D 2016 Seaweed-derived route to Fe_2O_3 hollow nanoparticles/N-doped graphene aerogels with high lithium ion storage performance *ACS Appl. Mater. Interfaces* **8** 7047–53

[31] Luebke M, Makwana N M, Gruar R, Tighe C, Brett D, Shearing P, Liu Z and Darr J A 2015 High capacity nanocomposite Fe_3O_4/Fe anodes for Li-ion batteries *J. Power Sources* **291** 102–7

[32] Luo J, Liu J, Zeng Z, Ng C F, Ma L, Zhang H, Lin J, Shen Z and Fan H J 2013 Three-dimensional graphene foam

supported Fe_3O_4 lithium battery anodes with long cycle life and high rate capability *Nano Lett.* **13** 6136–43
[33] Ma F-X, Wu H B, Xu C-Y, Zhen L and Lou X W 2015 Self-organized sheaf-like Fe_3O_4/C hierarchical microrods with superior lithium storage properties *Nanoscale* **7** 4411–4
[34] Ma T, Zhao Q, Wang J, Pan Z and Chen J 2016 A sulfur heterocyclic quinone cathode and a multifunctional binder for a high-performance rechargeable lithium-ion battery *Angew. Chem., Int. Ed. Engl.* **55** 6428–32
[35] Ming J, Li M, Kumar P and Li L-J 2016 Multilayer approach for advanced hybrid lithium battery *ACS Nano* **10** 6037–44
[36] Ren G, Hoque M N F, Liu J, Warzywoda J and Fan Z 2016 Perpendicular edge oriented graphene foam supporting orthogonal TiO_2(B) nanosheets as freestanding electrode for lithium ion battery *Nano Energy* **21** 162–71
[37] Ren Y, Liu Z, Pourpoint F, Armstrong A R, Grey C P and Bruce P G 2012 Nanoparticulate TiO_2(B): an anode for lithium-ion batteries *Angew. Chem., Int. Ed. Engl.* **51** 2164–7
[38] Ren Y, Wang J, Huang X and Ding J 2016 Enhanced lithium-ion storage performance by structural phase transition from two-dimensional rhombohedral Fe_2O_3 to cubic Fe_3O_4 *Electrochim. Acta* **198** 22–31
[39] Roberts A D, Li X and Zhang H 2014 Porous carbon spheres and monoliths: morphology control, pore size tuning and their applications as Li-ion battery anode materials *Chem. Soc. Rev.* **43** 4341–56
[40] Wan Y, Yang Z, Xiong G, Guo R, Liu Z and Luo H 2015 Anchoring Fe_3O_4 nanoparticles on three-dimensional carbon nanofibers toward flexible high-performance anodes for lithium-ion batteries *J. Power Sources* **294** 414–9
[41] Wang J, Gao M, Wang D, Li X, Dou Y, Liu Y and Pan H 2015 Chemical vapor deposition prepared bi-morphological carbon-coated Fe_3O_4 composites as anode materials for lithium-ion batteries *J. Power Sources* **282** 257–64
[42] Wei X, Tang C, Wang X, Zhou L, Wei Q, Yan M, Sheng J, Hu P, Wang B and Mai L 2015 Copper silicate hydrate hollow spheres constructed by nanotubes encapsulated in reduced graphene oxide as long-life lithium-ion battery anode *ACS Appl. Mater. Interfaces* **7** 26572–8
[43] Wu S, Wang Z Y, He C N, Zhao N Q, Shi C S, Liu E Z and Li J J 2013 Synthesis of uniform and superparamagnetic Fe_3O_4 nanocrystals embedded in a porous carbon matrix for a superior lithium ion battery anode *J. Mater. Chem.* A **1** 11011–8
[44] Wu Y, Wei Y, Wang J P, Jiang K L and Fan S S 2013 Conformal Fe_3O_4 sheath on aligned carbon nanotube scaffolds as high-performance anodes for lithium ion batteries *Nano Lett.* **13** 818–23
[45] Xiong Q Q, Tu J P, Lu Y, Chen J, Yu Y X, Qiao Y Q, Wang X L and Gu C D 2012 Synthesis of hierarchical hollow-structured single-crystalline magnetite (Fe_3O_4) microspheres: the highly powerful storage versus lithium as an anode for lithium ion batteries *J. Phys. Chem.* C **116** 6495–502
[46] Yang L, Liu W, Wang H, Liu S, Wang J and Chen J 2015 A low-cost and one-step synthesis of a novel hierarchically porous Fe_3O_4/C composite with exceptional porosity and superior Li^+ storage performance *RSC Adv.* **5** 102993–9
[47] Zhang H Y, Hu R Z, Liu H, Sun W, Lu Z C, Liu J W, Yang L C, Zhang Y and Zhu M 2016 A spherical Sn-Fe_3O_4@graphite composite as a long-life and high-rate-capability anode for lithium ion batteries *J. Mater. Chem.* A **4** 10321–8
[48] Zhang M, Lei D, Yin X, Chen L, Li Q, Wang Y and Wang T 2010 Magnetite/graphene composites: microwave irradiation synthesis and enhanced cycling and rate performances for lithium ion batteries *J. Mater. Chem.* **20** 5538–43
[49] Zhang M, Qu B, Lei D, Chen Y, Yu X, Chen L, Li Q, Wang Y and Wang T 2012 A green and fast strategy for the scalable synthesis of Fe_2O_3/graphene with significantly enhanced Li-ion storage properties *J. Mater. Chem.* **22** 3868–74
[50] Zhang W, Li X, Liang J, Tang K, Zhu Y and Qian Y 2016 One-step thermolysis synthesis of two-dimensional ultrafine Fe_3O_4 particles/carbon nanonetworks for high-performance lithium-ion batteries *Nanoscale* **8** 4733–41
[51] Zhao D, Qin J W, Zheng L R and Cao M H 2016 Amorphous vanadium oxide/molybdenum oxide hybrid with three dimensional ordered hierarchically porous structure as a high-performance li-ion battery anode *Chem. Mater.* **28** 4180–90
[52] Zhao H, Peng Z, Wang W, Chen X, Fang J and Xu J 2014 Reduced graphene oxide with ultrahigh conductivity as carbon coating layer for high performance sulfur@reduced graphene oxide cathode *J. Power Sources* **245** 529–36
[53] Zhao L, Gao M, Yue W, Jiang Y, Wang Y, Ren Y and Hu F 2015 Sandwich-structured graphene-Fe_3O_4@carbon nanocomposites for high-performance lithium-ion batteries *ACS Appl. Mater. Interfaces* **7** 9709–15